Concrete drying: effects of boundary conditions and specimen shape

Jérôme Carette, Farid Benboudjema, Georges Nahas, Kamilia Abahri, Aveline Darquennes, Rachid Bennacer

International RILEM Conference on Materials, Systems and Structures in Civil Engineering
Conference segment on Service Life of Cement-Based Materials and Structures
22-24 August 2016, Technical University of Denmark, Lyngby, Denmark

CONCRETE DRYING: EFFECTS OF BOUNDARY CONDITIONS AND SPECIMEN SHAPE

Jérôme Carette[(1,2)], Farid Benboudjema[(1)], Georges Nahas[(2)], Kamilia Abahri[(1)], Aveline Darquennes[(1)], Rachid Bennacer[(1)]

(1) LMT-Cachan / ENS Cachan / CNRS / Université Paris Saclay, Cachan, France
(2) IRSN, Fontenay-aux-Roses, FRANCE

Abstract
In the framework of the ODOBA project, representative structures in reinforced concrete are submitted to various types of durability distress, in order to have elements of knowledge on pathologies which could develop in the course of time. Among studied issues are the alkali-aggregate reaction (AAR) and the delayed ettringite formation (DEF), which appear after a large induction period, but develop then quickly, inducing irreversible structure damage. These issues are closely related to the water distribution and to the surrounding humidity. Controlling the processes of drying and wetting of concrete is of major importance in this regard. However, the mechanisms at their origin are currently not well established and modelled. This work is a preliminary study aiming at identifying the main mechanisms in play during drying-wetting cycles through a coupled experimental-numerical study of the humidity gradient inside concrete. In this paper, the drying of various concrete samples is cautiously studied through refined measurement of the mass loss and internal relative humidity distribution. Various sample sizes and shapes are tested. A simulation strategy is described, including the modelling of water vapour diffusion and liquid water permeation. The introduction of a boundary layer at the drying interface improves the mass variation prediction.

1. Introduction

In the framework of the pre-ODOBA ENSC/IRSN and ODOBA project of the IRSN (French Institut de Radioprotection et de Sûreté Nucléaire), representative structures of reinforced concrete will be built on the IRSN Cadarache nuclear research centre. In these structures will be developed pathologies of concrete such as swelling reactions (internal sulphate attack (ISA) and alkali-aggregate reaction (AAR)). The concrete used in the construction of these structures are chosen by equivalence to the concrete used in the studied nuclear facilities. These issues usually develop after a very long induction period (10 to 30 years). Unfortunately, after the onset of signs of swelling, development is very rapid with

consequences for the safety functions of these structures. These issues are highly dependent on the presence of water in the pore system of concrete. Therefore, control of the process of drying-wetting becomes an important parameter, which remains the object of scarce results in the literature. Indeed, there remain questions regarding the mechanisms involved. Thus, it is difficult to simulate the distribution of the water content in concrete models, which leads to difficulties in quantifying the deformation gradients due to the swelling reactions (ISA, AAR).
This work aims at identifying the main mechanisms in play during drying-wetting cycles through a coupled experimental-numerical study of the humidity gradient inside concrete. In this paper, the drying of various concrete samples is cautiously studied through refined measurement of the mass loss and internal relative humidity distribution. Various sample sizes and shapes are tested. A simulation strategy is described, including the modelling of water vapour diffusion and liquid water permeation [1, 2]. A limited amount of samples were tested in this study. In addition, many parameters of the model were determined by other authors on the same concrete. Therefore, this study must be considered as a preliminary methodology for the monitoring and simulating the drying of concrete rather. Additional ongoing tests will provide more information regarding further validation of the suggested model.

2. Experimental setup

2.1. Mix design

The tested concrete composition is referred to as B11 concrete. This concrete, which composition and major properties are shown in Table 1, is used because it is equivalent to the concrete actually used in French internal nuclear power plant vessels. In addition, it has been widely studied in previous studies [1] and its properties are therefore mostly known.

Table 1: (left) B11 mix design (right) B11 concrete main properties

	ρ [t/m^3]	**B11** [kg/m^3]	***w/c***	[-]	0.573
Cement (CEM II Airvault Calcia)	3.1	336	ρ	[t/m^3]	2.324
Sand (0/4)	2.572	740	**Slump**	[cm]	8-11
Aggregates (4/12,5)	2.57	303	**Porosity**	[-]	13.2-13.8
Aggregates (10/20)	2.57	752	f_c (28 days)	[MPa]	46.5
Water	1	193	f_t (28 days)	[MPa]	3.29
Superplasticizer (Plastiment HP)	$1.185\ 10^{-3}$	1.174	E (28 days)	[GPa]	31.34

2.2. Curing conditions

In order to submit all the concrete specimens to the same curing conditions (temperature T and relative humidity RH), à large storage bin was developed. The climatic chamber was

rejected for several reasons, the main one being the difficulty of limiting the forced convection on the faces subjected to drying, and of ensuring the uniformity of this phenomenon on all sides. The requirements of the storage bin are similar to those of a desiccator. It must be able to contain saline and be impermeable to air and moisture. In order to enable placing several temperature and relative humidity sensors inside the storage bin, sealing plugs were installed. The concrete samples were placed on a plastic honeycomb duckboard allowing maximized interaction between the salt solution and the ambient air. This setup is shown in Figure 1. The saturated salt solution was made using potassium carbonate in order to reach an ambient *RH* of close to 45%. The room temperature was controlled at 25°C.
The concrete samples were prevented from drying until the test started. The samples were submitted to drying more than two months after mixing. Due to the high *w/c* ratio of the B11 concrete, it can therefore be considered that the hydration reactions were completed, and that the auto-desiccation phenomenon could be neglected [3].

Figure 1: Experimental setup linked to the continuous measurement of *RH* and T sensors

2.3. Test setup

The experimental measurements consisted in mass loss measurements at regular intervals and in the continuous measurement of the internal relative humidity in concrete samples at various distances from the drying interface. Four sample geometries were considered:
- G1: 70x70x280mm prism, drying on the two opposite lateral faces,
- G2: 70x70x110mm prism, drying on the two opposite lateral faces,
- G3: 70x110mm cylinder, radial drying,
- G4: 70x70x110mm prism, drying on the four longitudinal faces.

For each of these geometries, the average drying radius (r_d) was computed as the ratio between the drying surface and the sample volume. This resulted in r_d of 0.14, 0.055, 0.0275 and 0.0175m for geometries G1, G2, G3 and G4 respectively.
The mass loss measurements were performed on 3 samples for G1, 2 samples for G2 and G3, and on 1 sample for G4. This study focuses on the first weeks after drying was initiated. The

relative humidity was measured at various distances from the drying interface on geometries G1, G2 and G3 according to the distribution shown in Figure 2.

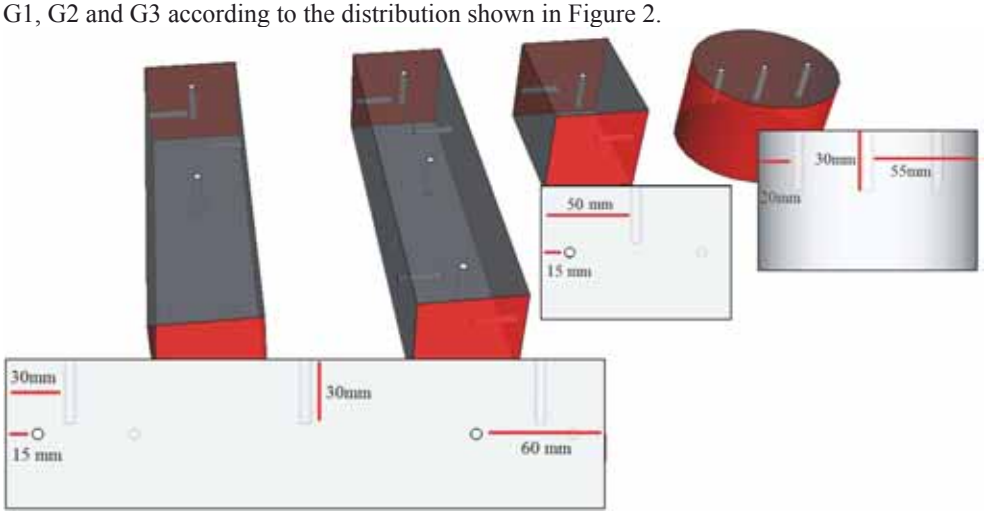

Figure 2: layout plan of *RH* sensors (sides submitted drying displayed in red)

3. Drying model

The drying model used in this study assumes that two mechanisms are at the origin of the water transport in the concrete: the diffusion of water vapour and the permeation of liquid water. If the concrete porous network is saturated, the latter mechanism is the predominant one, whereas for a low degree of saturation, the movement of water in the form of vapour diffusion cannot be neglected.

The liquid water flow can be expressed through Darcy's law, which relates the fluid mass flow through a medium to the pressure gradient of this fluid as expressed in the equation (1), where K_{eff} is the concrete effective permeability (s), p_c the capillary pressure (Pa), and J_l is the rate of liquid water flow (kg.m^{-2}.s^{-1}).

$$J_l = -K_{eff}\frac{\partial p_c}{\partial x} \tag{1}$$

According to the Kelvin equation, the relationship between the capillary forces and the relative humidity in concrete can be expressed as shown in equation 2, where M_w is the molecular mass of water (kg/mol), ρ_l is the liquid water density (kg/m^3), R is the gas constant (J.K^{-1}.mol^{-1}) and T is the temperature (K).

$$p_c = \frac{-\rho_l RT ln(hr)}{M_w} \tag{2}$$

In order to take into account the dependency of the water permeability to the degree of saturation, equation 3 can be used, where K_0 is the intrinsic water permeability of concrete in saturated conditions, μ_l is the water dynamic viscosity , and k_{rl} is the relative permeability. This latter term can be determined through the Mualem empirical relationship [4] shown in equation 4, where S_l is the saturation degree, p_{krl} is a fitting parameter. The relationship

between the degree of saturation and relative humidity is given by the van Genuchten equation [5] (equation 5), where a_{vg} and b_{vg} are two parameters that can be obtained by fitting experimental results of the desorption isotherm for the tested material.

$$K_{eff} = k_{rl}\frac{K_0}{\mu_l} \tag{3}$$

$$k_{rl} = {S_l}^{p_{krl}}\left(1-\left(1-{S_l}^{\frac{1}{a_{vg}}}\right)^{a_{vg}}\right)^2 \tag{4}$$

$$S_l = \left(1+\left(-b_{vg}ln(hr)\right)^{\frac{1}{1-a_{vg}}}\right)^{-a_{vg}} \tag{5}$$

Thus, equations 1-2 can be re-written as equation 6, while equations 3-5 allow to solve this equation for any given relative humidity.

$$J_l = -k_{rl}\frac{K_0\rho_l RT}{\mu_l M_w hr}\frac{\partial hr}{\partial x} \tag{6}$$

On the other hand, when the saturation degree decreases, pores are progressively not filled with water. This leaves space for a flow of water vapour (J_v, expressed in kg.m^{-2}.s^{-1}) due to the gradient of vapour pressure (p_v) between the inside of concrete and the ambient conditions according to Fick's law, as shown in equation 7.

$$J_v = -D_{eff}\frac{M_w}{RT}\frac{\partial p_v}{\partial x} \tag{7}$$

The effective diffusion coefficient in a porous medium (D_{eff}, expressed in m².s^{-1}) can be related to the degree of saturation, to the porosity (Φ) and to the diffusion coefficient of water in air (D_0) through the empirical Millington and Quirk relationship [6] expressed in equation 8. In equation 9, the relative humidity is related to the saturation vapour pressure p_{vs} and to the vapour pressure of water p_v.

$$D_{eff} = D_0.\Phi^{a_{mq}}.(1-S_l)^{b_{mq}} \tag{8}$$

$$hr = \frac{p_v}{p_{vs}} \tag{9}$$

The saturation vapour pressure is temperature dependent and can be determined by the Clausius-Clapeyron relationship (equation 10), where L_v is the heat of vaporisation of water (J/kg), T_0 is the reference temperature (273 K) and T is the air temperature (K). In the same way, the dependency of D_0 to temperature can be taken into consideration by equation 11.

$$P_{vs} = P_{atm}.e^{\frac{M_W.L_v}{R}\left(\frac{1}{T_0}-\frac{1}{T}\right)} \tag{10}$$

$$D_0 = 217.10^{-5}.\left(\frac{T}{T_0}\right)^{288} \tag{11}$$

From combining equations 6, 7 and 9, to the continuity equation, the equation that has to be solved for the moisture transport can be expressed as equation 12.

$$\Phi\frac{\partial S_l}{\partial hr}\frac{\partial hr}{\partial t} = \mathrm{div}\left[\left(K_{eff}\frac{\rho_l RT}{\mu_l M_v hr}+D_{eff}\frac{M_v P_v^{sat}}{\rho_l RT}\right)grad(hr)\right] \tag{12}$$

The modelling of drying requires the definition of adapted boundary conditions. Indeed, imposing the ambient relative humidity directly at the air-concrete interface is a possibility [1, 7]. However, such methodology does not take into account the presence of a boundary layer

of air at the air-concrete interface whose moisture content depends on the distance to the surface of concrete. This is important at the initiation of drying, because the high moisture content initially observed at the concrete surface gives rise to a boundary layer of air with high humidity at the air-concrete interface, which initially slows the drying kinetics. The thickness of this boundary layer strongly depends on the ambient conditions (air flow, temperature) and the material surface condition (surface roughness and moisture) [8]. Such boundary conditions can be more accurately represented by equation 13, in which J_{BC} represents the flow of water vapor at the air-concrete external interface, hr_s is the relative humidity at the interface and hr_e is the external air relative humidity. The value of h_{BC} is not well defined and can reach values from $1.x10^{-2}$ [8] to $8. x\ 10^{-7}$ [9] in natural conditions.

$$J_{BC} = -h_{BC}.(hr_s - hr_e) \tag{13}$$

4. Results and discussion

The ongoing tests related to the evolution of the humidity gradient measured by relative humidity sensors will not be presented in this section, which focuses on the mass loss. The results presented in Figure 3a indicate that when increasing the drying radius, the mass loss as a function of time is decreased. The curves representing the mass loss as a function of the square root of time (Figure 3b) present three successive stages. First, during the first hours after the drying starts, the mass loss increases with an accelerating rate. This stage, which is particularly marked in G4, lasts until approximately one day. Then, during the second stage, the mass loss increases as a linear function of the square root of time (which corresponds to the exact analytical simulation for semi-infinite media). This stage lasts longer as the drying radius increases. After more than one month, G1, which has the larger drying radius, still exhibits a linear evolution of the mass loss as a function of the square root of time. On the other hand, the second stage ends approximately after 3 days. Finally during the third stage, the mass loss increases with a decreasing rate. This stage occurs until the equilibrium between the concrete sample and the ambient air is reached, at which point no mass variations will be observed. These stages are described more thoroughly in following sections.

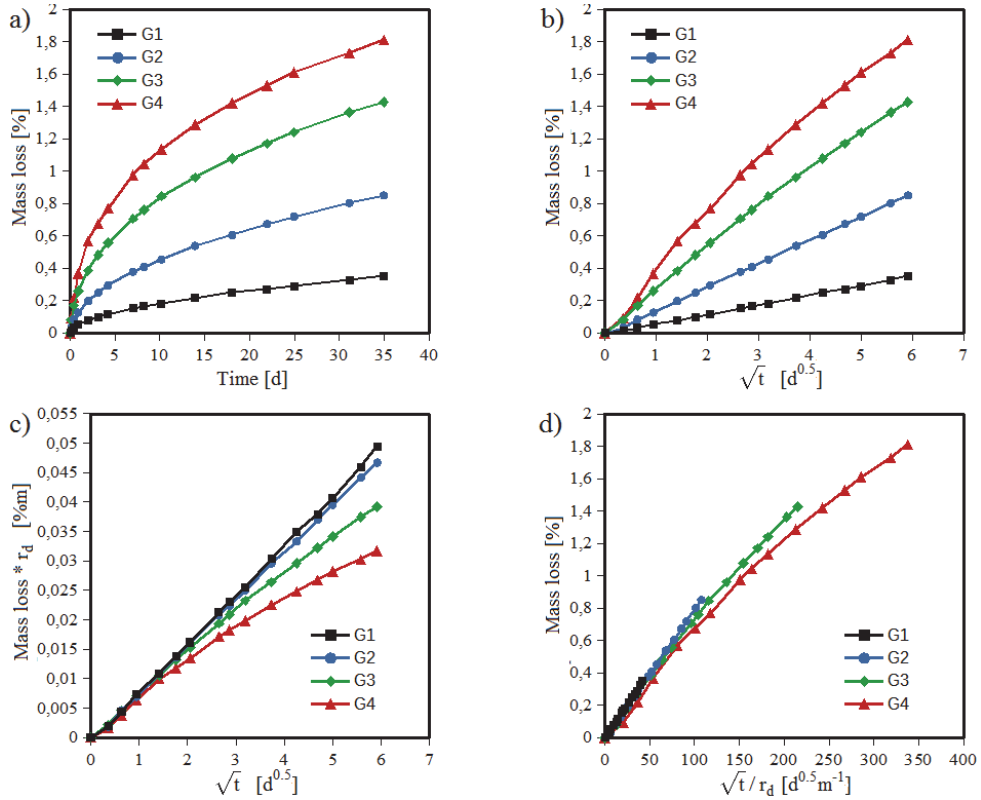

Figure 3: Various representations of the mass loss as a function of time and drying radius

4.1. Stage 1: initial drying and boundary layer

During the first hours and up to one day after the drying starts, the mass loss can be expressed as a non-linear function of the square root of time. This observation can be explained by the presence of a boundary layer of air at the concrete-air interface. Initially, all water extracted from the sample is present in the form of water vapour close to the concrete surface. This tends to increase the relative humidity of the ambient air, and therefore decrease the drying kinetics. Progressively, the water contained in the porosity in direct contact with the concrete surface evaporates. Due to the high diffusivity coefficient of water vapour in air in comparison with the concrete(equivalent) permeability and diffusivity, the relative humidity of the boundary layer decreases, until eventually reaching a value close to the actual ambient conditions.

In order to calibrate the value of parameter h_{CL}, preliminary tests are performed by measuring the relative humidity of the air against the drying surface through time. These measurements are shown in Figure 4a. Right after drying is initiated, the relative humidity at the surface is close to 80%. Then, progressively, it decreases until reaching a value of 55% at 5 days (120h). Initially, in order to correspond to these measurements, the best fit value of h_{BC} is situated

between 2.10^{-6} and 10^{-5}. However, progressively, the experimental dots tend to reach values closer to h_{BC} of 5.10^{-5}. One reason for this is that the exchange coefficient might change in time. This experiment indicates that as the saturation degree close to the surface decreases, the rate of exchange of water from the surface to the ambient air also decreases. Figure 4b shows the effect of changing h_{BC} on the mass loss during the first hours after drying. In the following simulations, a value $h_{BC}=10^{-5}$ is chosen.

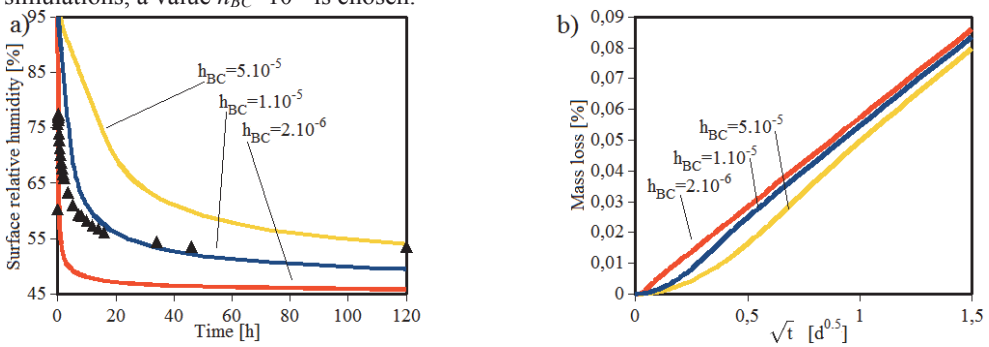

Figure 4: Effect of the exchange coefficient h_{BC} on the surface relative humidity, and comparison with experimental values (markers)

The results illustrated in Figure 5a show that the simulation strategy developed in section 3 allows representing the initial mass loss kinetics. The experiments are shown by dots, while the numerical simulations are represented by dashed lines. In these simulations, all parameters are kept constant, except for the geometry of the sample. The values of the parameters are all extracted from [1], except for the intrinsic permeability, which is fixed at $1.15x10^{-21}$. For G4, the value of the parameter h_{BC} is different than for other geometries. This is due to the specific drying surfaces of G4, one of which is the "top" side of the sample which was not in contact with the mould during setting and hardening.

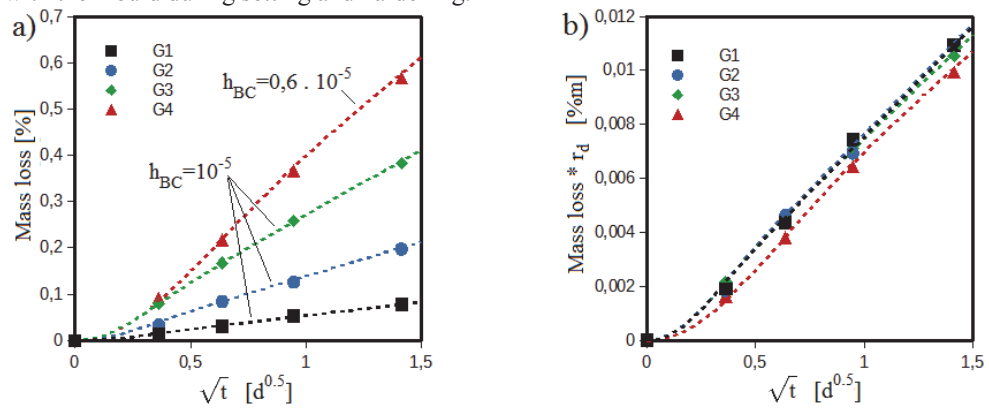

Figure 5: Initial mass loss during stage 1 (dots = experiments, dashed lines = simulations)

The surface roughness and porosity is therefore significantly different from all other surfaces, justifying a change in the exchange coefficient h_{BC}. In the same way, Figure 5b indicates that

except for G4, the sample size and shape effects on the initial mass loss can be accurately taken into consideration by multiplying the mass loss by the corresponding drying radius. However, this is only true if similar concrete and surface conditions are applied to all geometries.

4.2. Stage 2: main drying initiation

The second stage of drying consists in a linear increase of the mass loss as a function of the square root of time. The slope of this increase is related both to the concrete properties (porosity, permeability, diffusivity, …) and to the humidity gradient between the concrete and the ambient air. As for the first stage, the effect of the sample size and shape can be accurately taken into account by the drying radius. A higher drying radius induces a lower slope. By multiplying the drying radius by the slope of the mass loss curve during this second stage, all geometries present the same behaviour, as shown in Figure 4c and 4d. The end of this stage is not clearly defined, and probably occurs at a point where the effective permeability is significantly decreased in comparison with its initial value. This occurs when the overall humidity has significantly decreased in the whole sample, which could occur close to a specific mass loss. Further results should provide additional answers regarding this observation.

4.3. Stage 3: advanced drying and permeability decrease

As stated previously, the third stage consists in a significant decrease of the mass loss, resulting in a progressive decrease of the slope of the mass loss versus square root of time curve. At a given time, this phenomenon is more clearly observed in Figure 6a for geometries with lower drying radius. Indeed, G4 and G3 have already lost a significant amount of water, in contrast with G1 or G2.

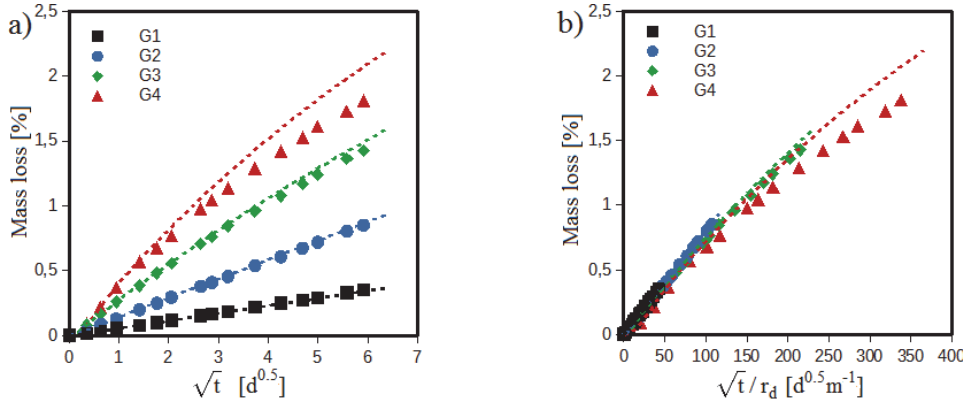

Figure 6: Whole mass loss curves (dots = experiments, dashed lines = simulations)

As for the first and second stage, the simulation captures this behaviour. However, as the mass loss increases, an overestimation of the simulation can be observed, especially when it overpasses 1%. This is due to the parameters expressed in equations 4, 5 and 8. These equations relate the relationship between saturation degree, relative humidity, and effective permeability and diffusivity. Indeed, all parameters from these equations were extracted from

another study [1]. Therefore, even if the same concrete was used, these equations should be adapted to this study. In particular, the decrease of effective permeability when decreasing the saturation degree should be more important. This point will be discussed further when longer term experiments have been performed on all sample sizes and shapes.

5. Conclusion and perspectives

Mass loss experiments on various specimen size and shape are performed. The model developed and used in [1] is improved by taking into account the boundary layer of air at the sample-air interface during drying. The curves of mass loss as a function the square root of time can be divided in three stages identified in this study: a non-linear acceleration initial stage, a linear drying initiation, and an advanced drying consisting in a decreased slope of the curve. These three stages can be accurately reproduced by the model, independently on the sample size and shape.
Further works are required in order to confirm the relevance of this model for longer term experiments, and for identifying mechanisms at the origin of the switch between the second stage and the thirst stage. Additional results regarding the relative humidity gradient inside the specimens will allow a mode complete description of these phenomena, as well as an improved strategy for identifying the parameters of the model. Finally, this validity of this model should be challenged with drying/wetting cycles experiments.

References

[1] Hilaire A., Etude des déformations différées des bétons en compression et en traction, du jeune au long terme : application aux enceintes de confinement, PhD Thesis, ENS Cachan, 2014
[2] Huang, Q.; Jiang, Z.; Gu, X.; Zhang, W. & Guo, B., Numerical simulation of moisture transport in concrete based on a pore size distribution model, Cem Conc Res , 2015, 67, 31-43
[3] Briffaut, M., Etude de la fissuration au jeune âge des structures massives en béton : influence de la vitesse de refroidissement, des reprises de bétonnage et des armatures, PhD Thesis, ENS Cachan, 2010
[4] Mualem, Y. (1976). A new model for predicting the hydraulic conductivity of unsaturated porous media. Water resources research, 12(3):513–522
[5] van Genuchten, M. A Closed-form Equation for Predicting the Hydraulic Conductivity of Unsaturated Soils. Soil Science Society of America Journal, 44(5):892–898, 1980
[6] Millington, R., Quirk, J. (1961). Permeability of porous solids. Transactions of the Faraday Society, 57:1200–1207
[7] Oxfall, M.; Johansson, P. & Hassanzadeh, M. Long-term hygrothermal performance of nuclear reactor concrete containments – Laboratory evaluations of measurement setup, in situ sampling, and moisture flux calculations, Cem and Conc Composites , 2016, 65, 128 – 138
[8] Zhang, J.; Wang, J. & Han, Y. Simulation of moisture field of concrete with pre-soaked lightweight aggregate addition, Construction and Building Materials , 2015, 96, 599 – 614
[9] Ožbolt, J.; Oršanić, F. & Balabanić, G. Modeling influence of hysteretic moisture behavior on distribution of chlorides in concrete, Cement and Concrete Composites , 2016, 67, 73 – 84